International Journal of Astrobiology 1 (4): 333–348 (2003) Printed in the United Kingdom
DOI: 10.1017/S147355040300123X

Laser wavelength selection for Raman spectroscopy of microbial pigments *in situ* in Antarctic desert ecosystem analogues of former habitats on Mars

Howell G.M. Edwards[1], Emma M. Newton[1], the late David D. Wynn-Williams[2], David Dickensheets[3], Chris Schoen[4] and Chelle Crowder[3]

[1]*Department of Chemical and Forensic Sciences, University of Bradford, Bradford BD7 1DP, UK*
e-mail: h.g.m.Edwards@bradford.ac.uk
[2]*British Antarctic Survey, Natural Environment Research Council, High Cross, Madingley Road, Cambridge CB3 0ET, UK*
[3]*Department of Computer & Electrical Sciences, University of Montana, Bozeman, Montana, USA*
[4]*Top Raman Inc. (Micron Optical Systems Ltd), Norfolk, Virginia, USA*

Abstract: The vital ultraviolet- (UV-) protective and photosynthetic pigments of cyanobacteria and lichens (microbial symbioses) that dominate primary production in Antarctic desert ecosystems auto-fluoresce at short wavelengths. We therefore use a long-wavelength (1064 nm) infrared laser for non-intrusive *in situ* Raman spectrometry of their ecologically significant compounds (especially pigments). To confirm that the power loss at this longer wavelength is justified to avoid swamping by background fluorescence, we compared Raman spectra obtained with excitation at 1064, 852, 830, 785, 633 and 515 nm. These are typical of lasers used for Raman spectroscopy. We analysed communities of the cyanobacterium *Nostoc commune* and the highly pigmented lichens *Acarospora chlorophana* and *Caloplaca saxicola*. These require screening compounds (e.g. pigments such as scytonemin in cyanobacteria and rhizocarpic acid in the fungal symbiont of lichens). They are augmented by quenching pigments (e.g. carotenoids) to dissipate the energy of free radicals generated by penetrating UV. We also analysed organisms having avoidance strategies (e.g. endolithic communities within translucent rocks, including the common cyanobacterium *Chroococcidiopsis*). These require accessory pigments for photosynthesis at very low light intensities. Although some organisms gave useable Raman spectra with short-wavelength lasers, 1064 nm was the only excitation that was consistently excellent for all organisms. We conclude that a 1064 nm Raman spectrometer, miniaturized using an InGaAs detector, is the optimal instrument for *in situ* studies of pigmented microbial communities at the limits of life on Earth. This has practical potential for the quest for biomolecules residual from any former surface life on Mars.

Accepted 1 October 2002

Key words: Antarctic, laser Raman spectroscopy, Mars analogues, microorganisms, pigments.

Introduction

Ecological role of pigments

Solar radiation is the prime energy source for surface microbial colonists in lithic habitats (lithosols and rocks) of Antarctic deserts. Use of this energy requires photosynthetic pigments to harness visible photons, the most important being chlorophyll. However, concurrent exposure to ultraviolet (UV) radiation also damages pigments themselves (Rajagopal *et al.* 2000) and other functional biomolecules such as DNA (Buma *et al.* 1995), enzymes and other protein (Chauhan *et al.* 1998). Protection against this damage requires survival strategies that involve pigments with three different roles: (1) screening pigments such as cyanobacterial scytonemin, which filter out UV-A and UV-B (and potentially UV-C, although this is screened out by the atmosphere); (2) anti-oxidant pigments such as β-carotene that quench the energetic free radicals and singlet oxygen that are generated by intrusive UV radiation; and (3) accessory pigments such as cyanobacterial phycocyanin. This supports an avoidance strategy that enables photosynthetic organisms to shelter within habitats such as endolithic communities (Wynn-Williams 2000) and function at very low light levels.

These pigments give distinctive diagnostic Raman spectra, and their longevity within the recent and distant fossil biochemical record makes them good biomarkers for early life on the Earth and potential former life on Mars

(Wynn-Williams *et al.* 1999; Wynn-Williams & Edwards 2001). Antarctic desert communities are valuable analogues of putative former Martian habitats. Using pigmented Antarctic microbial communities such as cyanobacterial mats and UV-exposed lichens as biological targets, laser Raman spectroscopy has been proven as a potential tool for remote analysis for relict pigments (Wynn-Williams & Edwards 2000). The choice of the laser for this analysis is crucial to avoid autofluorescence of the pigments that would swamp the weak Raman signal.

Suitable Antarctic communities for evaluating this approach contain photosynthetic bacteria (green and purple sulphur and non-sulphur bacteria), such as the Chlorobiaceae, Chromatiaciae and Rhodospirillaceae (Burke & Burton 1988). However, the dominant organisms in these lithosol and sediment habitats are cyanobacteria (Vincent *et al.* 1993) and to a lesser extent eukaryotic algae (Broady 1996). In drier epilithic habitats on rocks and endolithic endolithic habitats inside them, symbiotic lichen microbial associations containing fungi with either algae or cyanobacterial symbionts (Friedman 1982; Friedman *et al.* 1988; Kappen 1993) and associated bacteria (Siebert *et al.* 1996).

UV-protective pigments

Three distinct groups of pigments and other compounds are central to protective strategies.

1. UV-screening compounds such as the pigments scytonemin in cyanobacterial sheaths and parietin in lichens and the mycosporine-like amino acids (MAAs) within the cells of various organisms (Cockell & Knowland 1999).
2. Quenching compounds such as carotenoid pigments found in most photosynthetic organisms (Jahnke 1999).
3. Accessory pigments such as cyanobacterial phycocyanin that absorb PAR at very low levels (MacColl 1998) thus supporting shade-adaptation and the avoidance strategy of minimizing exposure to UV radiation.

Because of their functional need to absorb either UV radiation or PAR, UV-screening compounds have distinctive structures. These typically include rings such as the tetrapyrrole ring of chlorophyll, the aromatic ring quadrant of scytonemin (Prouteau *et al.* 1993) and aromatic rings linked by a *trans* unsaturated chain in β-carotene. These structures give unique laser-Raman spectra, the corroborative bands of which constitute a 'fingerprint' for spatial detection of a given compound within undisturbed communities and strata *in situ*. The spatial distribution of the UV-absorbing anthraquinone pigment parietin has been analysed *in situ* using Raman spectroscopy of UV-exposed Antarctic epilithic lichen communities within the ozone hole (Edwards *et al.* 1998). Similarly, the Raman spectrum of sheath scytonemin has been shown in intact cyanobacterial desert crust communities and in pure cultures (Wynn-Williams *et al.* 1999). A certain amount of UV will penetrate exposed cells. Some of this will be absorbed internally by mycosporine-like amino acids, for which the Raman spectra have recently been determined (Newton 2001).

UV-quenching pigments

Free radicals and singlet oxygen produced by the action of the UVR are quenched by pigments such as β-carotene. Carotenoids have distinctive Raman spectra that are conspicuous in photosynthetic microbial communities from diverse habitats (Edwards *et al.* 1998; Holder *et al.* 2000; Wynn-Williams *et al.* 2000). They are found in all photosynthetic microbes (bacteria and cyanobacteria) and certain chromogens such as *Deinococcus radiodurans*. β-carotene has conspicuous Raman vibrational bands that permit its diagnosis in whole lichens (e.g. *Xanthoria elegans*), despite the presence of many other bands from their complex algal–fungal symbiosis (Wynn-Williams *et al.* 2000).

Accessory photosynthetic pigments

Avoidance strategies are available to shade-adapted microbes, which can produce accessory pigments to augment photon capture by their primary chlorophyll-based photosynthetic system. These organisms include endolithic communities in translucent Beacon Sandstone of the Trans-Antarctic Mountains (Nienow *et al.* 1998), and benthic stromatolites on bottom sediments of ice-covered lakes in the McMurdo Dry Valleys and other Antarctic desert regions (Wharton 1994).

Longevity of pigments

Degradation products of photoproductive and photoprotective pigments often have a high longevity. Porphyrins derived from chlorophyll (Huseby *et al.* 1996) and aryl isoprenoids from carotenoids (Damste & Koopmans 1997) are found in the fossil record from up to three billion years ago. Accessory pigments, including cyanobacterial phycocyanin and phycoerythrin, have been obtained from Arctic permafrost that was over a million years old (Erokhina *et al.* 1998). Raman spectra of ancient biomolecules might therefore provide evidence of former photosynthetic microbial activity in now desertified rocks and soils in Antarctica. This approach could then be extended to analogous habitats on Mars, which had more water available during its Hesperian period (McKay 1997; Wynn-Williams & Edwards 2000).

This paper describes the relative merits of different laser wavelengths for Raman spectrometry of pigments *in situ* within Antarctic microbial communities of relevance to the search for evidence of biomolecules from putative former life on Mars. We hypothesized that 1064 nm excitation would be optimal for minimizing autofluorescence whilst not jeopardizing power loss at the longer wavelength.

Materials and methods

Selection of lasers for Raman spectroscopy of pigments

Raman spectroscopy provides a unique spectral 'fingerprint' for any molecule, depending on the vibrational state of its component moieties and their mutual interactions (Edwards & Newton 1999). Often, there are key components that give a clear and distinctive vibrational band, giving an indication of the potential eco-physiological function of the compound

https://doi.org/10.1017/S147355040300123X Published online by Cambridge University Press

Table 1. *Sample locations and habitats*

	Acarospora chlorophana	*Caloplaca saxicola*	*Nostoc commune*	Cryptoendolithic lichen	*Chroococcidiopsis sp.*
Location	Football Saddle, Northern Victoria Land	Crater Cirque, Northern Victoria Land	Mars Oasis, Alexander Island	East Beacon, McMurdo Dry Valleys	Balham Valley/ Barwick Valley
Latitude	72° 31′		71° 53′ S	77° 50′ S	77° 20′ S
Longitude	169° 46′		68° 14′ W	160° 53′ E	161° 05′ E
Altitude (m asl)	*ca.* 800	*ca.* 800	*ca.* 50	2200	
Distance to coast (km)	*ca.* 10	*ca.* 10			
Aspect, facing	S	N		N	N
Substratum, exposure and climatic factors	Pitted substratum comprising alkalibasalt, trachyandesite and phonolite. Sheltered micro-habitats on southern slope of saddle	McMurdo volcanics comprising alkalibasalt, trachyandesite and phonolite. Sheltered northeast-facing slope	Aquatic and loosely settled on silt. Sheltered to south and west, within zone of enhanced UV-B levels during ozone depletion	Sedimentary orthoquartzite sandstone. Exposed ridge, iron-stained outcrop	Sedimentary orthoquartzite sandstone. Sheltered valley, little iron staining
Moisture (range)	Not known. Rock surface	Not known. Rock surface	Fringes of melt pond	0.13–1.12% dw	~1%
Habitat	Crustose	Epilithic, crustose	Aquatic and littoral	Endolithic	Endolithic

in the microbial community. An example is the aromatic ring quadrant in scytonemin, where the cyanobacterial UV-screening pigment gives a strong vibrational Raman band at wavenumber 1590 cm^{-1} (Edwards *et al.* 1999). However, this band is also conspicuous in other microbial screening pigments such as the anthraquinones parietin and atranorin found in epilithic Antarctic desert lichens that contain the same aromatic ring quadrant (Edwards *et al.* 1998). It is therefore necessary to have a set of corroborative bands, which provide a spectral description of the compound in terms of its component moieties and their interaction with each other. The four strong bands at 1590, 1549, 1323 and 1172 cm^{-1} are a sound diagnosis for the presence of scytonemin in cyanobacterial communities (Wynn-Williams *et al.* 1999).

A Raman spectrum therefore consists of bands that must be assigned to certain moieties, based on the experience learned from analysing known compounds and close derivatives. The advantage of this concept is that there are no preconceived ideas of what a compound is, which is a prerequisite for extending this analytical approach to the surface of Mars (Wynn-Williams & Edwards 2000). It is highly suitable for analysing the spatial distribution of unknown biochemicals *in situ* within microbial communities with respect to their eco-physiological function rather than merely a summary of their composition (Russell *et al.* 1998). The conspicuous 1590 cm^{-1} band indicates that the molecule is likely to have UV-absorbing properties, the exact specification of which will be fine-tuned by other moieties in the compound to adjust the wavelengths absorbed. This is potentially how microbes adjusted (and still adjust) to changing solar radiation climates. A UV-absorbing molecule would become the basis for mutational changes and selective pressure for the community to keep pace with changes or become extinct.

Raman spectroscopy therefore provides an approach not only to obtaining an inventory of key functional and diagnostic biomolecules, but also to predict and confirm the role of key biomolecules in survival and evolution of photosynthetic microbial communities on early Earth. It also permits the study of present conditions with changing stresses such as enhanced UV-B within the Antarctic ozone hole, and has predictive potential for conditions on early Mars.

Table 1 presents the location and habitat information for the samples used in this comparison study. A range of Antarctic species were chosen, encompassing both epilithic and endolithic lichens and cyanobacterial communities. The two epilithic lichen samples are commonly found in Antarctic maritime and coastal regions: *Acarospora chlorophana*, from Football Saddle and *Caloplaca saxicola* from Crater Cirque, both in Northern Victoria Land. The former was a deep yellow coloured crustose lichen, whilst the latter had a rich orange–red colour. An endolithic lichen from East Beacon and an endolithic cyanobacteria (*Chroococcidiopsis sp.*) from Balham Valley were also studied. An intertidal mat of *Nostoc commune* from Mars Oasis was included as an example of a surface-living cyanobacterial community.

https://doi.org/10.1017/S147355040300123X Published online by Cambridge University Press

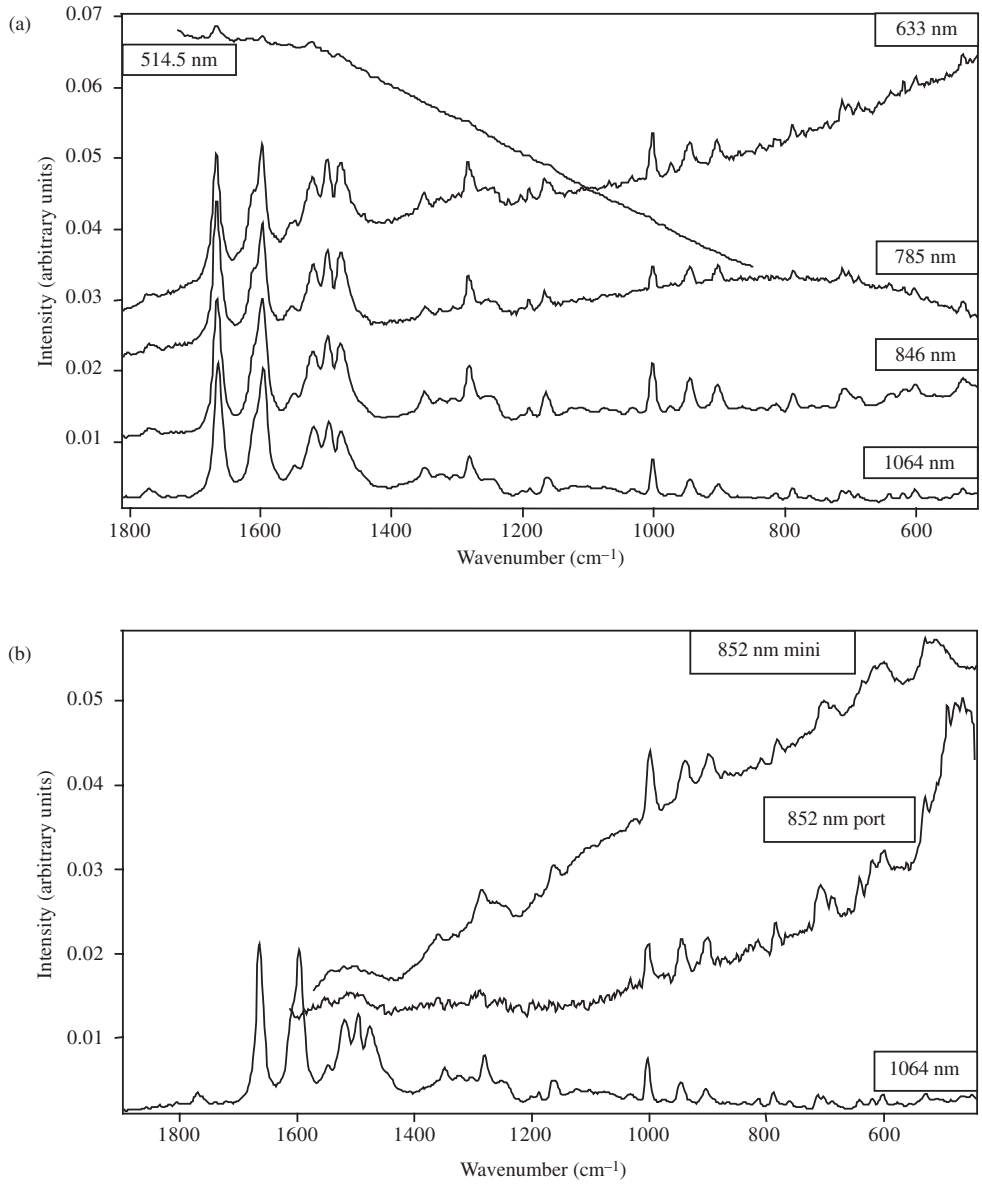

Fig. 1. (a) Stack plot of Raman spectra of *Acarospora chlorophana* collected using laser excitations of 514.5, 633, 785, 846 and 1064 nm. (b) Stack plot of Raman spectra of *Acarospora chlorophana* collected using laser excitations of 852 nm: miniature system (mini), portable system (port) and 1064 nm.

For exposed samples (lichens and mats), three replicates were scanned directly without preparation. For the endolithic communities, three replicate rock samples were fractured vertically to expose the community. The 10 mm profile was divided into up to five zones, where present and point spectra were collected at three replicate spots per zone. Spectra of the surface crust and the zone of iron accumulation were obtained using the Fourier transform- (FT-) Raman spectrometer in macroscopic mode with a spot diameter of 100 μm at the surface of the sample. Compilation spectra given in the figures are based on representative spectra that were recorded in triplicate per zone. The relative proportions of chemical compounds detected were determined from the spectra but absolute values were not determined.

Excitation at 1064 nm with a bench-top Raman spectrometer

Spectra excited by a laser at 1064 nm wavelength were recorded using a Fourier-transform Bruker IFS66 (Bruker IR Analytische GmbH, Karlsruhe) instrument and FRA 106 Raman module attachment with a 350 mW Nd/YAG laser and a liquid-nitrogen-cooled germanium detector. For spectroscopy of rock profiles and surface crusts, this was coupled via a television camera to a Raman microscope with a $\times 40$ objective giving a spot diameter of *ca.* 40 μm at the sample. The power level was set as low as possible to minimize sample degradation whilst optimizing signal quality, and was typically 20 mW. Between 4000 and 10 000 scans (accumulated at *ca.* 2 scans s^{-1}) were needed to obtain good spectra at

https://doi.org/10.1017/S147355040300123X Published online by Cambridge University Press

4 cm^{-1} resolution with wavenumbers accurate to ± 1 cm^{-1} or better. The total energy input for 4000 scans was therefore *ca.* 40 J, and exhaustive trials with a variety of endolithic samples showed degradation during scanning to be negligible.

Excitation at 852 nm with a portable Raman spectrometer ('*port*')

The Raman Solution 852 system (Detection Limit Inc., Wyoming, USA) employed a 150 mW distributed Bragg reflector (DBR) frequency-stabilized diode laser giving 60 mW at the sample. The 852 nm output wavelength was the longest currently available in conventional charge-coupled device- (CCD-) based Raman systems. The spectrograph had an $f/2$, 1200 lines mm^{-1} grating, TE-cooled Kodak 0400 CCD with a wavenumber spectral range of 250–2400 cm^{-1} and a resolution of 7–8 cm^{-1}. The detector probe was fibre-optically coupled and measured $11.5 \times 5.0 \times 3.8$ cm^3, weighing 0.4 kg. Its removable lens assemblies allowed for working distances ranging from <3 mm to >10 cm. The total mass of the laser, spectrograph and CCD of this portable instrument was <9 kg.

Excitation at 852 nm with a miniature Raman spectrometer ('*mini*')

Spectra excited by an 852 nm laser were obtained with a micro-miniaturized confocal microscope and Raman spectrometer (CMaRS-852) system (specification mass <1 kg), under development by Montana State University and Detection Limit Inc. with NASA funding for potential Mars landers. Its small probe head (<100 cm^3) contains the confocal microscope and Raman filters, fibre-coupled to the laser light source and spectrometer housed in an electronics bay. The confocal microscope (imaging at video rates of 30 frames s^{-1}) comprises a silicon micro-electromechanical (MEMS) bi-axial scanning mirror, precision-molded aspheric lenses and piezoelectric focus control. The light source for both components is an 852 nm distributed Bragg reflector diode laser. Rayleigh scattered light is detected to form the confocal image, while Raman-shifted light is separated by a Raman filter set and detected with a dispersive CCD-based compact spectrometer. The spectral resolution is 8 cm^{-1} over a range from 400 to 1800 cm^{-1}. Raman spectra may be obtained over a variable field of view by controlling scanning in the microscope, from a minimum spot size of 1 μm to full field of 250 μm × 250 μm. The 852 nm spectrum was obtained from a laboratory prototype of the miniature instrument while scanning a field measuring 60 μm × 100 μm with an incident power of 20 mW for a duration of 300 s and a total energy dose of 6 J.

Excitation at 785, 633 and 514.5 nm

A Renishaw System 100 Raman spectrometer was used to obtain Raman spectra in the visible (633 and 514.5 nm) and near infrared (785 nm) regions, comprising an Olympus BH2 imaging microscope and a Peltier-cooled (-70 °C) CCD detector with an array of 576×384 pixels. Typical powers of about 50 μW with a 100× microscope objective lens were used to provide a specimen 'footprint' of about 2 μm diameter. Spectra were recorded with a spectral resolution of 4 cm^{-1} and collection times of up to 30 s per scan to enhance the signal-to-noise ratio. The instrument was calibrated using a silicon film and setting the strong Raman band to 520 cm^{-1}. Notch filters with a cut-off about 150 cm^{-1} from the Rayleigh line were used.

During the course of our study, an opportunity was afforded to record some spectra using systems similar to those above and experimental diode lasers operating further into the near infrared at 830 and 846 nm. Specimen spectra at these wavelengths are provided in the stack plots, where appropriate.

Results

Acarospora chlorophana

This yellow crustose lichen from Football Saddle, Antarctica, gave the most informative Raman spectra with numerous diagnostic peaks for comparisons between different laser excitations in this study. Good quality spectra were obtained from all systems except the 514.5 nm excitation instrument, which resulted in strong fluorescence, swamping the weaker Raman spectra. Figs 1(a) and (b) show stack plots of the spectra obtained from the range of instruments, separated into two plots for ease of comparison, with the FT-Raman spectra (1064 nm) shown in both. For clarity, only the range *ca.* 1800–500 cm^{-1} is shown, since the ν(CH) region at *ca.* 3000 cm^{-1} is only visible in the spectra from the 1064 and 633 nm instruments. Both aromatic and aliphatic ν(CH) modes are identifiable in the spectra. As with all stack plots in this section of work, the spectra are not overlaid with the same *y*-axis limits, since the scales vary significantly, e.g. from 0 to 0.2 arbitrary units in the spectrum collected at 1064 nm and from 0 to 6000 arbitrary units in that collected at 633 nm. However, the spectra have been roughly normalized so that the most intense bands in each are similar in intensity, for comparison purposes. Table 2 summarizes the wavenumber positions and approximate vibrational assignments from these spectra, for all instruments.

The strong bands, which can be seen in all the spectra at approximately 1665 and 1596 cm^{-1}, are most likely due to the yellow pigment rhizocarpic acid, the former being assigned to the ν(C═O) amide mode and the latter a ν(C═C) aromatic mode. These bands are unfortunately outside the range of the miniature systems that are restricted by the lack of sensitivity of CCD detectors to infrared radiation. The next intense band of interest is the *ca.* 1520 cm^{-1} band assigned to the ν(C═C) stretch of a carotenoid, most probably β-carotene, with a corroborative ν(C—C) component at *ca.* 1160 cm^{-1}. The former is the uppermost in a group of three bands that are clearly visible in all spectra except those from the portable and miniature systems and the green excitation, which is highly fluorescent. The other two features are characteristic of calcium oxalate in both monohydrate and dihydrate states; ν(CO) modes at approximately 1496

https://doi.org/10.1017/S147355040300123X Published online by Cambridge University Press

Table 2(a). *Raman wavenumbers and approximate vibrational assignments for* Acarospora chlorophana (*range 750–3100 cm*$^{-1}$)

Excitation wavelength (nm)							
1064	852 port	852 mini	846	785	632.8	514.5	Approximate assignment
3063 m					3062 vw		ν(CH) aromatic
2934 s, br					2923 vw, br		ν(CH)
1771 mw			1770 w	1768 w	1769 w		ν(C═O) cyclic ester (RA*)
1665 vs			1666 vs	1666 vs	1666 vs	1666 s	ν(C═O) amide (RA)
1610 s, sh			1610 s, sh	1610 s, sh	1609 s, sh		ν(CCH) aromatic
1596 vs			1597 vs	1598 vs	1596 vs	1596 m	ν(C═C) aromatic (RA)
1548 mw			1548 mw	1550 mw	1550 mw		Ring stretches, RA aromatic
1519 s			1519 s	1520 s	1518 s	1520 ms, br	ν(C═C) β-carotene
1497 s			1497 s	1498 s	1498 s	1499 m	ν(CO) Ca oxalate monohydrate
1476 s			1478 s	1477 s	1477 s	1480 mw	ν(CO) Ca oxalate dihydrate; ν(C═C) aromatic (RA)
	1360 w	1360 w					$\delta(CH_2)$
1349 mw	1341 vw		1350 mw	1350 mw	1347 w		$\delta(CH_2)$
		1334 w					
1281 ms	1288 mw	1285 ms	1281 ms	1281 ms	1282 ms	1281 w	$\delta(CH_2)$
1188 vw			1189 vw	1189 vw	1190 w		Ring breathing
1163 mw		1163 m	1165 m	1166 mw	1166 mw	1159 vw	ν(C—C) β-carotene
1031 vw	1031 w		1033 w	1034 vw			ν(C—O) RA
1002 ms	999 s	998 vs	1002 ms	1001 m	1001 m		ν(C—C) ring breathing, ar. RA
945 mw	944 ms	939 s	945 m	944 m, br	944 m, br		$\rho(CH_2)$ RA
902 mw	903/898 s	899 s	902 m	903 m	903 m, br		ν(CC) Ca oxalate monohydrate
	815 mw	809 mw	813 vw				ν(CC) aliphatic
787 w	783 ms	781 m	786 mw	788 w	787 mw		Substratum
760 vw			760 vw				δ(CH) aromatic, (RA)

* Rhizocarpic acid.
Signal strength: vs = very strong; s = strong; mw = medium; w = weak; vw = very weak; br = broad band; sh = sharp band.

Table 2(b). *Raman wavenumbers and approximate vibrational assignments for* Acarospora chlorophana (*range 200–750 cm*$^{-1}$)

Excitation wavelength (nm)							
1064	852 port	852 mini	846	785	632.8	514.5	Approximate assignment
	725 w						
711 w			708 mw	713 w	713 mw		
702 vw	706 s, br	701 ms, br		703 w	703 w		
687 vw	687 m		688 w, sh	697 vw	687 w		δ(CH) aromatic, (RA*)
640 vw	639 ms	636 mw	637 w	639 vw	641 w		Ring deformation, aromatic
619 vw	619 m	616 m	616 w	619 w	618 vw		ν(CCO) ring
599 w	597 m, br	600 m	601 mw	601 w	603 w		ν(CCO) ring
527 w	528 ms	529 ms, br	527 mw	529 w	529 w		δ(CCO) Ca oxalate monohydrate
508 vw, sh		511 ms, br	510 w, sh				Substratum
	489 s						
	477 s						Substratum
464 vw	463 ms		465 w, sh				α-quartz
449 vw			447 mw	447 w	450 w		
406 vw		406 ms, br	408 w				Substratum
206 vw							α-quartz

* Rhizocarpic acid.
Signal strength: vs = very strong; s = strong; mw = medium; w = weak; vw = very weak; br = broad band; sh = sharp.

and 1476 cm^{-1}, respectively. The latter may also have some contributions from the 1463 cm^{-1} band of calcium oxalate monohydrate, which can be perceived as a slight shoulder in the 1064 and 846 nm spectra and more clearly in the 785 nm spectrum. Previous work on *Acarospora sp*. in our laboratory has suggested that Antarctic species contain more calcium oxalate dihydrate than monohydrate (Holder *et al*. 2000); however, this is not the case with this sample. The relative intensities of the characteristic bands are comparable, indicating that similar concentrations are present.

https://doi.org/10.1017/S147355040300123X Published online by Cambridge University Press

Table 3. *Raman wavenumbers and approximate vibrational assignments for* Caloplaca saxicola

Excitation wavelength (nm)			
1064	852 mini	830	Approximate assignment
3069 w			ν(C═CH) aromatic
3036 w			ν(CH) aromatic
2918 s, br			ν(CH_3) asymmetric
1672 s		1672 w	ν(C═O) conjugated, free; parietin
1631 w, sh			ν(C═O) conjugated, H-bonded; parietin
1612 ms			ν(C═C) aromatic; parietin
1553 s		1554 mw	ν(C═C) aromatic; parietin
1520 vs			ν(C═C) β-carotene
1477 w, sh			Ring stretch coupled with (OH); parietin
1450 m			Ring stretch; parietin
1380 ms			Ring stretch, in plane/ν(C—O) phenyl
1370 ms			Ring stretch, in plane/ν(C—O) phenyl
1322 w			Ring stretch, in plane; parietin
1276 vs		1277 ms	Ring stretch, in plane; parietin
1254 ms, sh		1256 m	ν(C—O) aromatic ether; parietin
1198 mw			Ring stretch, C—C chelate; parietin
1180 w			Ring stretch, C—C chelate; parietin
	1161 mw, br		α-quartz
1156 s			ν(CC) β-carotene
1137 w, sh			δ(C–CH), in plane; parietin
1105 w			δ(C–CH), in plane; parietin
	1080 vw		α-quartz
	1062 vw		α-quartz
1004 mw			ν(CC) ring breathing; ar./β-carotene
926 s		927 ms	δ(C–H) out of plane; parietin
	794 mw, br		α-qurtz
	693 mw		α-quartz
631 mw		633 m	Skeletal deformation; parietin
611 mw		611 m	Skeletal deformation; parietin
572 m		572 ms	Skeletal breathing; parietin
519 m			?; parietin
465 w, sh	470 vs*	467 m, sh	?; parietin/*α-quartz
458 s		459 ms	δ(C═O), in plane; parietin
416 mw		423 m	?; parietin
397 m	405 mw*	400 m	Skeletal deformation; parietin/*α-quartz
	367 w		α-quartz
241 w		240 m, br	?; parietin

Signal strength: vs = very strong; s = strong; mw = medium; w = weak; vw = very weak; br = broad band; sh = sharp.

The region between 1400 and 1200 cm^{-1} contains several δ(CH_2) modes, which are present at varying intensities in all spectra.

A group of three bands that can also be identified in all spectra, except the green, are at *ca.* 1000, 940 and 900 cm^{-1}. These are assigned to ν(C—C) ring breathing and ρ(CH_2) of rhizocarpic acid and possibly the ν(CC) stretch of calcium oxalate monohydrate. Many of the bands in the lower-wavenumber region are due to the rock substratum on which the *Acarospora chlorophana* is growing, namely trachyandesite with a high concentration (>60%) of silica.

Caloplaca saxicola

Table 3 presents the wavenumber positions and approximate vibrational assignments for the spectra that had visible bands. Figs 2(a) and (b) show stack plots of the spectra obtained from the range of instruments, again separated into two plots for clarity, with the FT-Raman spectrum shown in both. Again, the range *ca.* 1700–300 cm^{-1} is used, since the ν(CH) region around 3000 cm^{-1} is only visible in the spectrum from the 1064 nm instrument.

Caloplaca saxicola did not produce spectra of comparable quality to those of *Acarospora chlorophana*. However, as predicted from previous studies, the best quality results were gained using the 1064 nm spectrometer. The spectrum from the 830 nm instrument, although noisy and displaying some signs of sample heating, did show bands corresponding to the lichen pigment, parietin. The bands were broad, but the positions matched those in the FT-Raman spectrum very closely. The baseline of the spectrum from the 785 nm spectrometer was similar to that of 830 nm, but there were no bands discernible. The 633, 514.5 nm and portable and miniature instruments gave very noisy spectra with no discernible bands, showing only the effects of fluorescence (and possible heating of the sample in the case of the latter). The spectrum from the miniature system shows bands corresponding to α-quartz, although most are quite broad and so appear to be slightly shifted from the positions of those

https://doi.org/10.1017/S147355040300123X Published online by Cambridge University Press

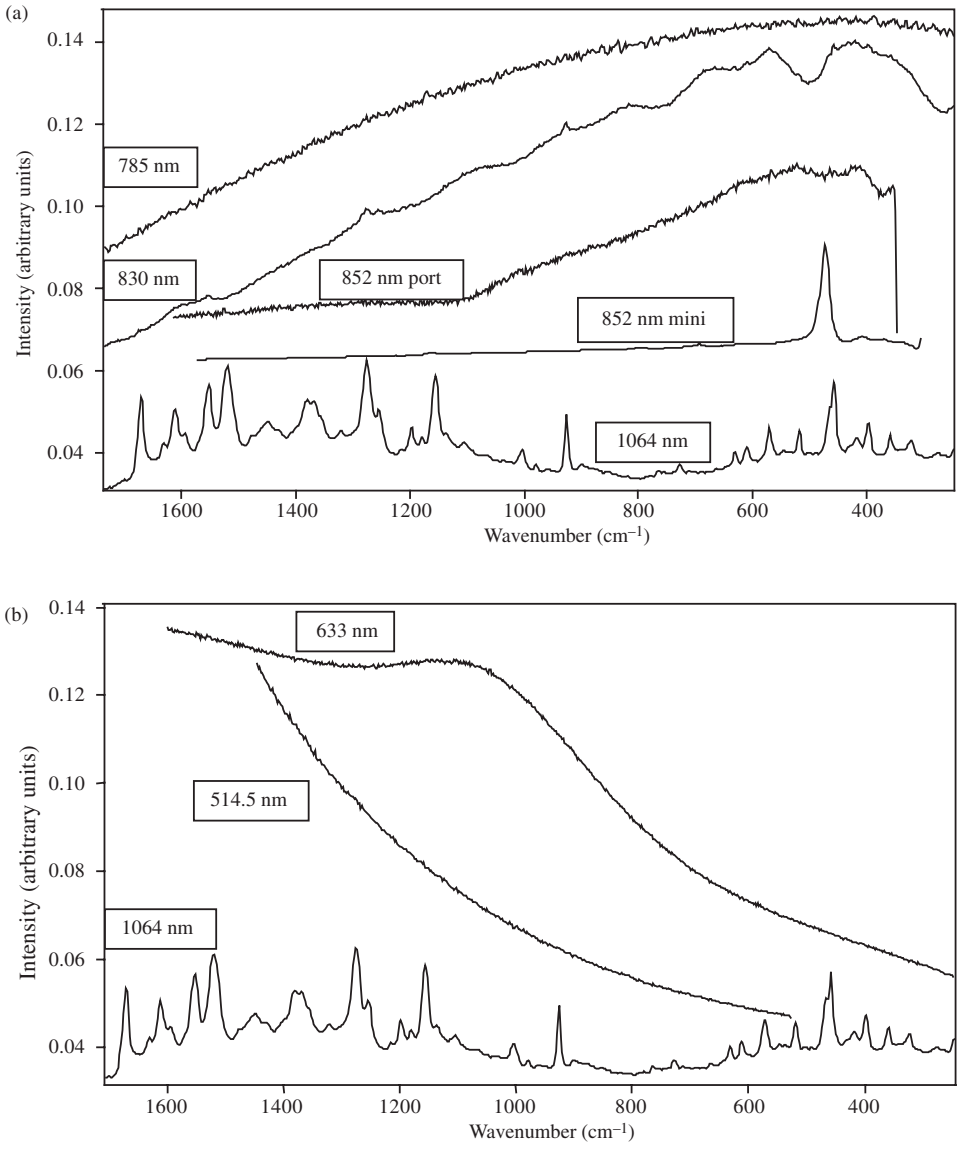

Fig. 2. (a) Stack plot of Raman spectra of *Caloplaca saxicola* collected using laser excitations of 785, 830 and 852 nm; portable (port) and miniature (mini) and 1064 nm. (b) Stack plot of Raman spectra of *Caloplaca saxicola* collected using laser excitations of 633, 514.5 and 1064 nm.

in pure α-quartz. These bands are from the rock substratum on which the lichen was growing.

Several characteristic bands of the anthraquinone parietin can be identified in the 1064 and 830 nm spectra. For example, strong bands at 1672 and 926 cm^{-1}, show the free ν(C═O) and δ(C—H) modes, respectively. β-carotene is present in relatively high concentrations, as demonstrated by the intense ν(C═C) band at 1520 cm^{-1} and the ν(C—C) band at 1156 cm^{-1}.

Nostoc commune

The *Nostoc commune* sample was a very dark green/black coloured mat, which dried under the laser. However, repeated sampling showed that the Raman spectra did not change despite exposure to the laser. Table 4 presents the wavenumber positions and approximate vibrational assignments for the spectra that had visible bands. Fig. 3 shows a stack plot of the spectra obtained from the range of instruments. There are no spectra from the 830 and 852 nm instruments, owing to sample burning. The range *ca.* 1700–400 cm^{-1} is presented, as there are no bands of interest outside this range.

Again the 1064 nm system gave the clearest spectrum despite some interference from fluorescence even at this high wavelength. The major bands can be attributed to the UV-protective pigment scytonemin, as described in previous work (Edwards *et al.* 1999). Although they are not evident on the scale used for the comparative stack plots shown, the characteristic scytonemin bands at *ca.* 1596, 1550, 1323 and 1173 cm^{-1} can also be identified in the 514.5 nm spectrum. Another important compound that can be detected in the 514.5 nm Raman spectra is β-carotene, which comprises some 39% of the total carotenoid content of *Nostoc commune*

https://doi.org/10.1017/S147355040300123X Published online by Cambridge University Press

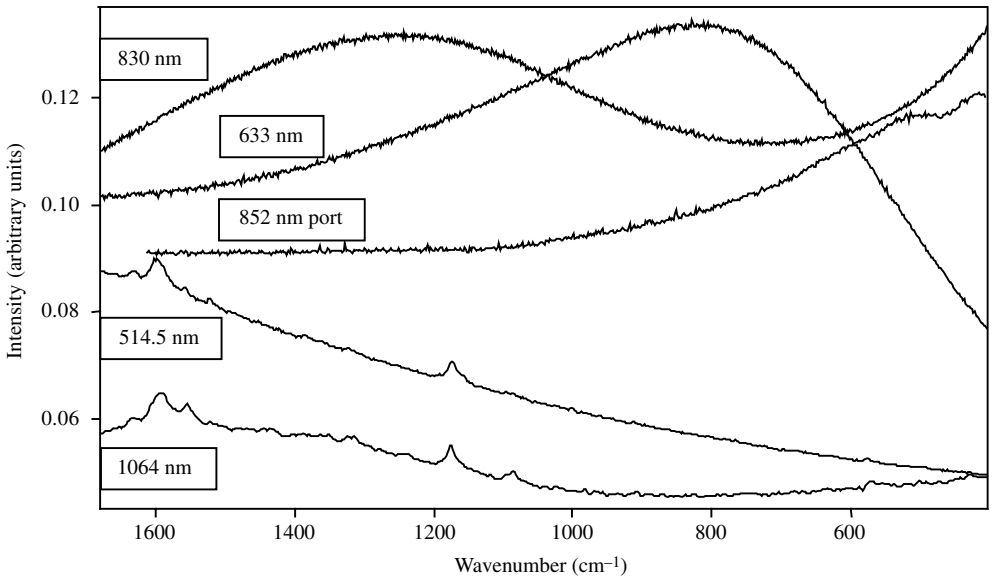

Fig. 3. Stack plot of Raman spectra of *Nostoc commune* collected using laser excitations of 514.5, 633, 785 and 852 nm portable system (port) and 1064 nm.

Table 4. *Raman wavenumbers and approximate vibrational assignments for* Nostoc commune

Excitation wavelength (nm)		Approximate assignment
1064	514.5	
1797 ms		
1708 mw	1709 w, br	ν(C═O)*
1631 mw, sh	1635 m	ν(C═O) conjugated *trans**
1590 s, br	1597 s, br	ν(CCH) aromatic ring quadrant*
1555 m	1558 m	ν(CCH) p-disubstituted aromatic ring*
1521 w	1523 mw	ν(N═C—C═C) ring mode*/ν(C═C) β-carotene
1443 w, d		δ(C═CH)*
1434 w, d	1385 mw, br	ν(CCN) indole ring*
1323 w, d	1325 w	ν(C═N) indole ring*
1315 w, d		Chlorophyll *a*
1175 ms	1173 ms	ν(C═C—C═C) trans configuration*
1159 w, sh	1158 m, sh	ν(CC) ring breathing pyrrole*/ν(C—C) β-carotene
1096 mw, sh	1097 w	δ(COH) phenolic*
1086 m	1084 w	
	1003 w	β-carotene
570 w, br	576 w, br	δ(CCN) aromatic ring indole system*
502 vw		δ(CCCO) twist*

* Scytonemin bands, assigned after Edwards *et al.* 1999.
Signal strength: vs = very strong; s = strong; mw = medium; w = weak; vw = very weak; br = broad band; sh = sharp.

(Stransky & Hager 1970). The strength of the bands could be due to resonance enhancement, since they are very weak in the 1064 nm spectrum. A band of medium intensity in the 1064 nm spectrum, at 1086 cm^{-1}, is indicative of $\nu(CO_3^{2-})$ and is a characteristic band of calcium carbonate, which would not be expected in this sample. However, it is impossible to identify any other corroborative bands due to the noise in the spectrum and so this band has remained unassigned in this study. The spectra from the 785, 633 and 852 nm Raman systems were noisy with curved baselines, indicating fluorescence and also thermal heating of the sample, particularly in the case of the mini-Raman spectrum.

Endolithic lichens

As this sample had several distinct biological and geological layers, it was investigated using Raman microscopy. This enabled spectra to be accumulated from each layer down a vertical transect (see Fig. 4), without disturbing the community. The miniature system was not able to produce any spectra for this sample and the portable system showed only substratum information. As previously described, the 830 nm instrument was aligned to produce a laser line, rather than a spot, at the sample surface. For this reason, it was only possible to obtain spectra from the crust and the black lichen layers, as the other zones were too narrow to obtain a spectrum that did not overlap an adjacent zone. Wherever possible, each separate layer is discussed and stack-plotted individually, due to the large number of spectra collected. The stack plots do not show the ν(CH) region, as bands were only visible in the spectra from the organic layers, collected by the FT instrument. Table 5 presents the Raman wavenumbers and approximate assignments for the biological layers. The substratum information is incorporated into each biological layer to avoid repetition, since α-quartz bands were visible in all spectra from the FT-Raman instrument. Fig. 5(a) shows a stack plot of spectra from the rock substratum and accumulation layers of the endolith, collected at several wavelengths. These areas produced essentially the same spectra and so the best quality spectrum is used for each instrument, with the exception of 1064 nm, for which both spectra were of equal quality and that of the crust is shown.

https://doi.org/10.1017/S147355040300123X Published online by Cambridge University Press

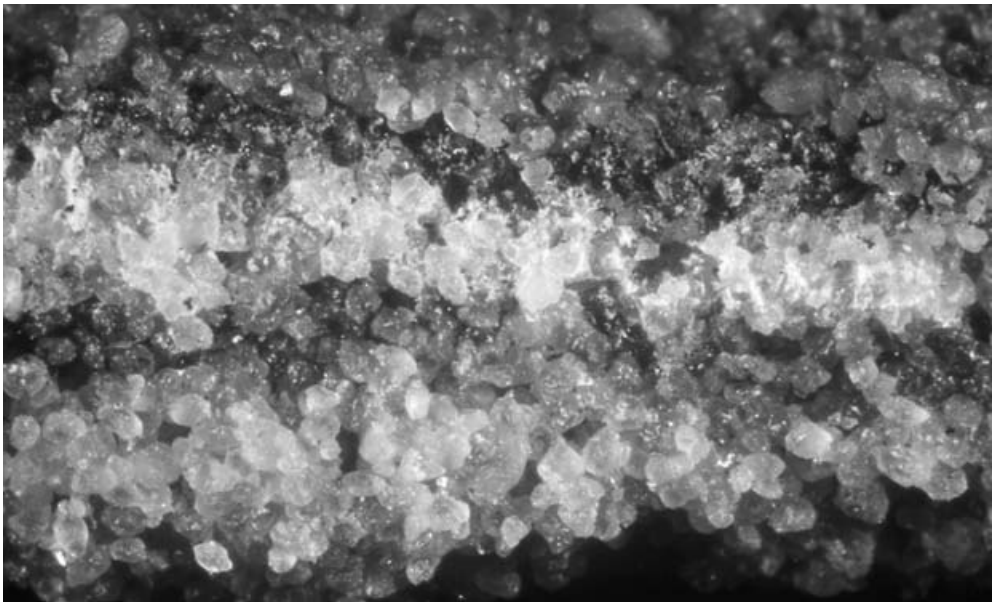

Fig. 4. Vertical profile of an endolithic microbial community in Beacon sandstone, having an iron-stained crust, a black lichen upper layer, with a hyaline lichen mid-layer and an innermost layer of algae and/or cyanobacteria. The section shown is 8 mm.

The substratum bands are entirely attributable to α-quartz, owing to its strong scattering ability. Indeed, the only features visible in the portable Raman spectrum are the most intense of the quartz bands at 465 cm^{-1}.

The spectra collected from the black lichen layer are presented in Fig. 5(b). Useable spectra were obtained from all instruments except the 785 nm instrument, which was affected by fluorescence, with the spectrum showing no bands. The spectrum from the 1064 nm instrument incorporates rock substratum bands, i.e. α-quartz bands, but the other spectra are free from substratum interference. Calcium oxalate dihydrate can be seen in all the spectra (except for 785 nm), with the ν(CO) band at approximately 1477 cm^{-1}, the intensity varying between weak and medium. The 1064 nm spectrum also has weaker bands characteristic of the monohydrate form of calcium oxalate; ν(CO) bands at 1490 and 1463 cm^{-1}. The former band can also be seen in the 830 nm spectrum, as a medium to weak shoulder on the stronger dihydrate band. This agrees with the work of Russell (1997), where the dihydrate form was found in the black lichen layer of several endolithic lichens. It has been postulated that the different hydration states are a form of water conservation (Russell *et al*. 1998).

A weak band in the 1064 nm spectrum at 1523 cm^{-1} has been assigned tentatively to the ν(C═C) band of β-carotene. Since the ν(C—C) mode is the strongest one in the β-carotene spectrum, there are no corroborative bands to confirm the presence of this pigment in the black lichen layer. Chlorophyll *a* can be seen in all the spectra as a relatively strong, broad feature, around 1320 cm^{-1}. There is a set of bands that appear in all the spectra at approximately 1625, 1561 and 1395 cm^{-1}, which are most probably due to the pigmentation in the layer. They are similar to the bands of other lichen substances, such as parietin, atranorin and gyrophoric acid. There are other bands in the 1064 and 830 nm spectra, at *ca*. 922 cm^{-1}, which are also reminiscent of anthraquinone modes of parietin and emodin. Although none of the previously analysed lichen substances are an exact match for the bands found in this lichen, it is thought that they are likely to be due to lichen pigmentation.

Fig. 5(c) shows a stack plot of spectra collected from the white lichen layer. Although weak α-quartz bands can be identified in the spectra from the green and 785 nm excitations, detail can only be ascertained in the 1064 nm spectrum. Along with the ubiquitous α-quartz bands, there are a number of conspicuous organic modes. In contrast to the black lichen layer, calcium oxalate is present only in the monohydrate form, with ν(CO) bands at 1490 and 1462 cm^{-1}, also found by Russell (1997). Chlorophyll *a* can be seen as a broad feature around 1320 cm^{-1}, but there are no bands to indicate the presence of β-carotene in this layer. There are as yet unassigned bands at 1661, 1632, 1281, 1001, 895, 883, 558 and 530 cm^{-1}, which are thought to be due to a lichen acid or pigment. Our work on lichen substances (Newton 2001) indicates a strong resemblance to the *para*-depside compounds, such as atranorin and gyrophoric acid. Both occur commonly in lichens, including those species thought to have endolithic growth forms (Nienow *et al*. 1988), such as *Lecanora* and *Lecidea*.

The spectra collected from the green algal layer of the endolithic lichen are shown in Fig. 5(d). A weak band at 460 cm^{-1} is the only visible band in the red excitation spectrum. Spectra from both the 1064 and 514.5 nm systems reveal the presence of β-carotene. Again it is thought that the strength of the signal in the latter is due to resonance enhancement. Although the ν(C—C) band of β-carotene is obscured by the strong α-quartz band at 1160 cm^{-1} in the

https://doi.org/10.1017/S147355040300123X Published online by Cambridge University Press

Table 5. *Raman wavelengths and approximate vibrational assignments for the white and black lichen layers and algal zone of the endolithic lichen*

Excitation wavelength (nm)							
White zone	Black zone				Algal zone		Approximate assignment
1064	1064	830	633	514.5	1064	514.5	
2939 ms	*ca.* 2900 w, br				2938 ms		ν(CH_2) antisymmetric
2881 ms					2883 ms		ν(CH_3) symmetric
2848 m, sh	2848 w, sh				2850 m, sh		ν(CH_2) symmetric
	1793 m, br						
1661 mw, br							Lichen substance
1632 w, sh	1623 m, br	1631 m	1625 ms, br	1627 ms, br			Lichen substance
	1561 m, br	1563 m, br	1570 mw, sh	1562 m, sh			Lichen substance
	1523 w				1526 m	*1524 mw*	ν(C═C) β-carotene
1490 vw	1492 mw, sh	1500 mw, sh			1486 mw, sh		ν(CO) calcium oxalate monohydrate
	1478 m	1475 m	1477 mw, br	1477 w	1474 m		ν(CO) calcium oxalate dihydrate
1462 mw	1463 m				1463 m		ν(CO) calcium oxalate monohydrate
		1448 w		1450 w	1444 mw, sh		
	1394 vw	*ca.* 1400 m, br	1393 w, br	*ca.* 1395 mw, br			Lichen substance
1319 m	1320 ms, br	1314 vs, br	1325 w, br	*ca.* 1330 mw, br	1320 m, vbr		Chlorophyll *a*
1281 mw, sh							
		1255 s, sh		1248 m, br			Lichen substance
1230 w	1230 vw, sh	1221 m, sh			1227 w		α-quartz
1160 m	1160 m						α-quartz
					1159 m	*1156 mw*	ν(C—C) β-carotene
1081 mw, d	1082 mw, d				1081 mw, d		α-quartz
1064 mw, d	1064 mw, d				1064 mw, d		α-carotene
1001 w				1012 m	1003 w		ν(C—C) aromatic
				998 mw, sh			
	921 vw	924 mw					Lichen substance
895 w							
883 w							
806 mw, d	807 mw, d	809 m, sh			807 mw, d		α-quartz
795 mw, d	796 mw, d	788 ms			796 mw, d		α-quartz
696 w	695 w				696 w		α-quartz
		688 ms, br					
				664 m			
558 mw		560 ms, br					Lichen substance
530 w							Lichen substance
		500 s, br					Lichen substance
464 vs	*464 vs*				*464 vs*		α-quartz
393 m	393 m				394 m		α-quartz
		360 m, br					
355 m	355 m				355 m		α-quartz
263 m	263 m				263 m		α-quartz
		245 mw, br					
206 s	*206 s*				*206 s*		α-quartz

Signal strength: vs = very strong; s = strong; mw = medium; w = weak; vw = very weak; br = broad band; sh = sharp.

1064 nm spectrum, it can be perceived visually by a slight shift towards the low-wavenumber region and has been confirmed by peak deconvolution. The weak band at 1003 cm^{-1} has been identified as a β-carotene mode, due to the absence of other strong organic substances. Both forms of calcium oxalate are present in similar amounts. Again, a very broad feature at 1320 cm^{-1} is assigned to chlorophyll *a*.

Endolithic cyanobacteria (*Chroococcidiopsis*)

This sample had two distinct areas for analysis; a green-coloured cyanobacterial layer and the rock substratum. Figs 6(a) and (b) present the spectra collected from both zones. The Raman wavenumbers and approximate vibrational assignments can be seen in Table 6. The spectra from the 633 and 785 nm instruments were masked by fluorescence and the portable Raman spectrum showed only the more intense α-quartz bands at *ca.* 467, 400 and 691 cm^{-1}. No spectrum was obtained by the miniature instrument. The 830 nm instrument produced a good quality spectrum from the substratum, showing several bands characteristic of α-quartz, but the spectrum from the cyanobacterial layer was not as good, due to a large

https://doi.org/10.1017/S147355040300123X Published online by Cambridge University Press

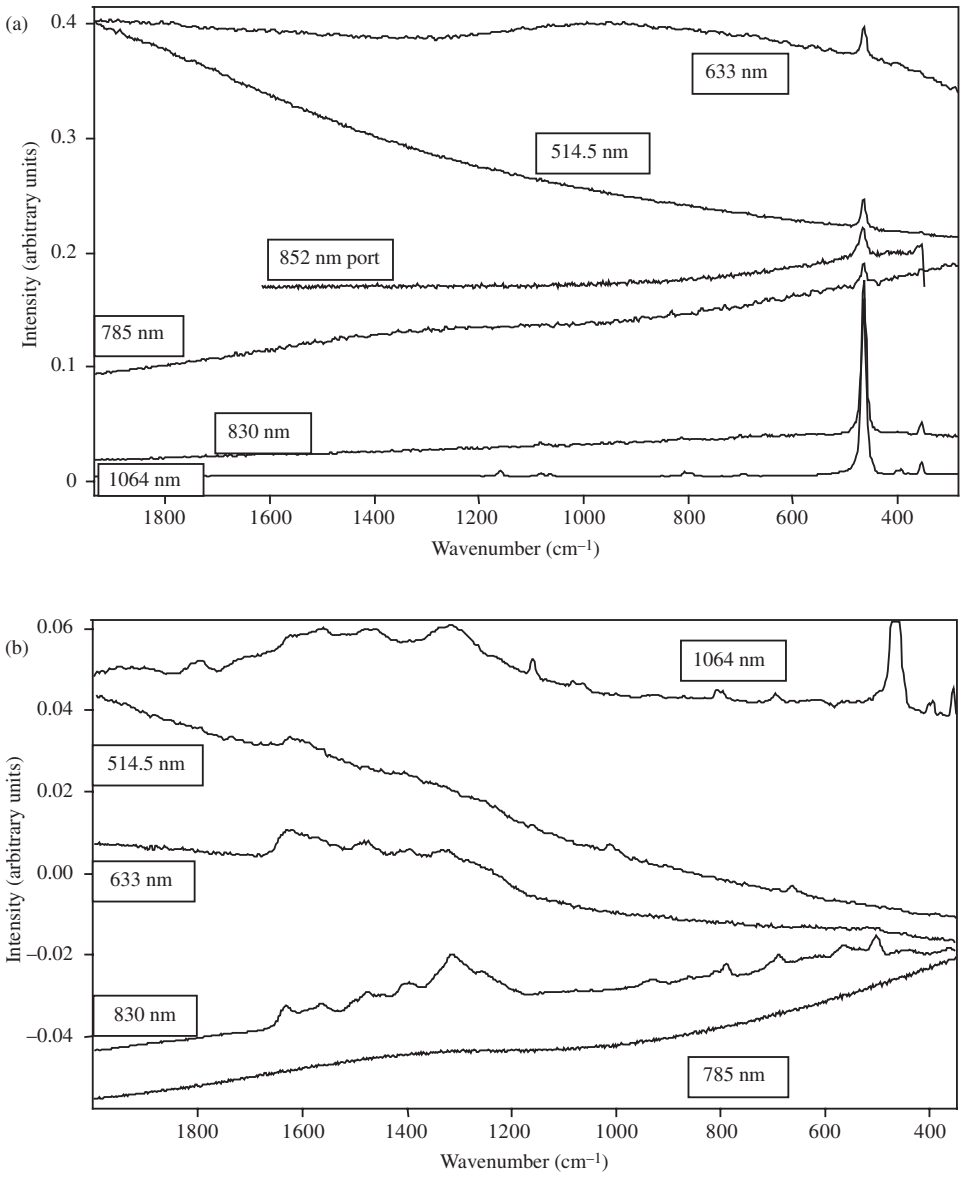

Fig. 5. (a) Stack plot of Raman spectra of endolithic lichen rock substratum collected using laser excitations of 514.5, 633, 785, 830 and 852 nm portable system (port) and 1064 nm. (b) Stack plot of Raman spectra of an endolithic black lichen layer collected using laser excitations of 514.5, 633, 785, 830 and 1064 nm. (c) Stack plot of Raman spectra of an endolithic white lichen layer collected using laser excitations of 514.5, 633, 785 and 1064 nm. (d) Stack plot of Raman spectra of endolithic green algal layer collected using laser excitations of 514.5 nm, 633 m, 785 nm and 1064 nm.

fluorescence background obscuring the majority of the spectrum.

The 1064 nm instrument produced good quality spectra from both zones. The only unequivocally identifiable organic compound was β-carotene, with its characteristic bands at 1515 and 1155 cm^{-1} being visible in the spectra from both the 1064 and 514.5 nm systems. Again, band deconvolution was used to confirm the presence of the 1155 cm^{-1} band in the FT spectrum as it was masked by the α-quartz mode at 1160 cm^{-1}. A weak band around 1006 cm^{-1} was assigned to ν(C—C) aromatic stretches. Weak bands at 1633, 1585 and 1450 cm^{-1} in the 1064 nm spectrum are as yet unassigned, but are similar to bands found in the endolithic lichen spectra.

Conclusions and discussion

Infrared laser excitation at 1064 nm is optimal for Raman spectroscopy of pigments and other biomolecules in photosynthetic organisms because of its minimal induction of autofluorescence that masks the weaker Raman signal. Its application to a wide range of materials of microbiological and astrobiological materials shows its great potential for spatial analysis of intact communities within their

https://doi.org/10.1017/S147355040300123X Published online by Cambridge University Press

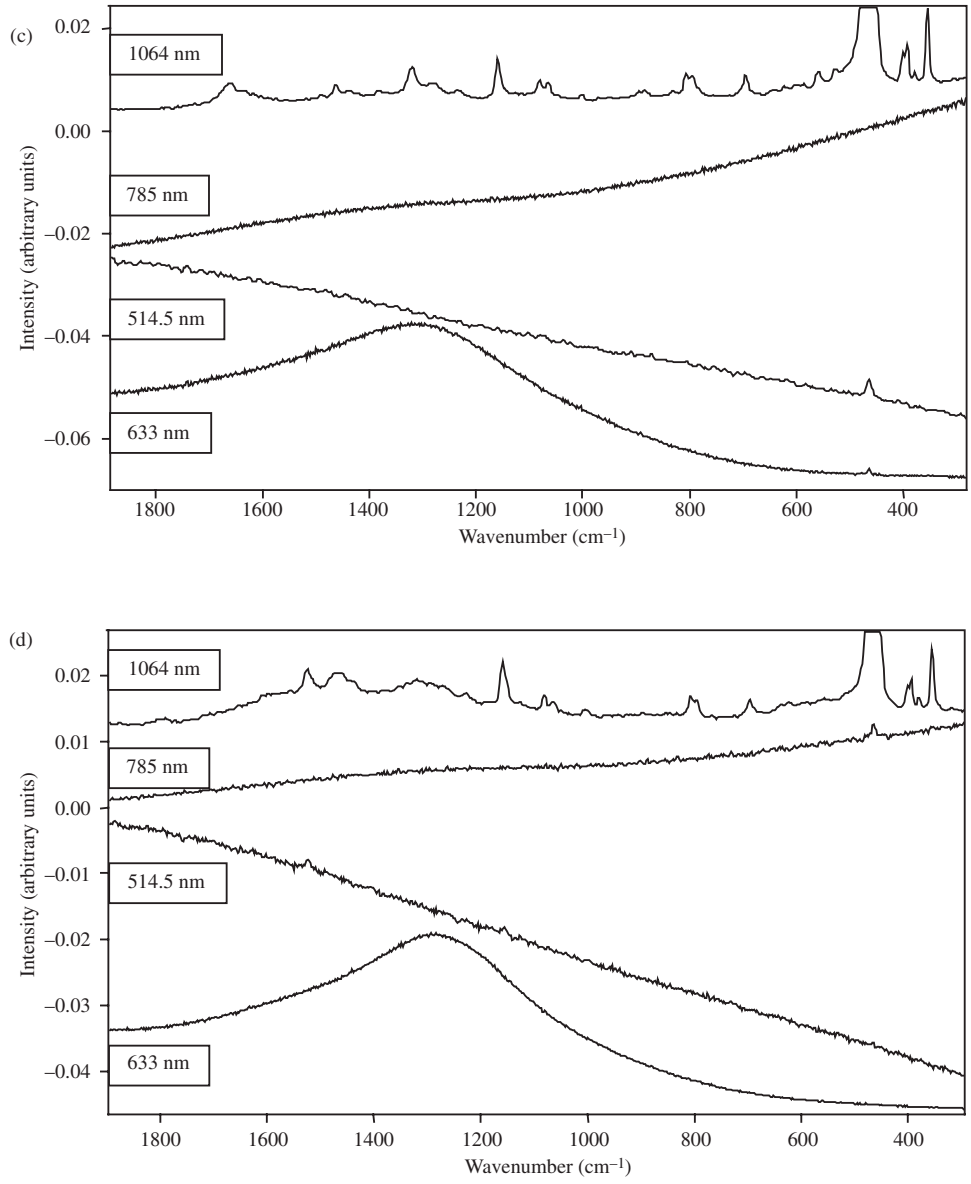

Fig. 5. (Cont.)

microhabitats to determine the stratification and organization of their functional structure (Edwards *et al.* 1998; Russell *et al.* 1998; Wynn-Williams *et al.* 1999; Holder *et al.* 2000; Wynn-Williams & Edwards 2000).

Fluorescence and heating resulting from short-wavelength excitation makes the highly energetic short-wavelength systems used for Raman spectroscopy of mineral materials (Haskin *et al.* 1997; Wang *et al.* 1999) generally inappropriate for delicate biomolecules in photosynthetic microbial primary producers. Moreover, these instruments developed for planetary missions to date have focused on surface measurements rather than on the potential of fibre-optic probes for side-scan analysis of buried strata in palaeolakes, which are a primary target for biomolecule detection (Wynn-Williams *et al.* 2001). However, it is not necessarily the shortest wavelengths that give the poorest Raman spectrum because, when excited near an electronic absorption band, pigments can give selectively strong Raman signals in a resonance effect. However, absorption of the laser radiation can also result in heating and degradation of the sample. Higher energy input at shorter wavelength gives a stronger Raman signal, but also more fluorescence. Pigments fluoresce optimally at specific excitation wavelengths rather than merely shorter ones, but those wavelengths are all less than 1064 nm. Ultraviolet Raman spectroscopy can be used for biomolecules (Hashimoto *et al.* 1997), but its high energy content tends to thermally degrade microbial materials.

The conspicuous cut-off in the Raman spectrum at *ca.* 400 cm^{-1} in 852 nm portable and miniature systems precludes the detection at *ca.* 3000 cm^{-1} of key organic signatures of amide groups and –CH and methyl groups. These are of fundamental relevance to the detection of carbohydrates

https://doi.org/10.1017/S147355040300123X Published online by Cambridge University Press

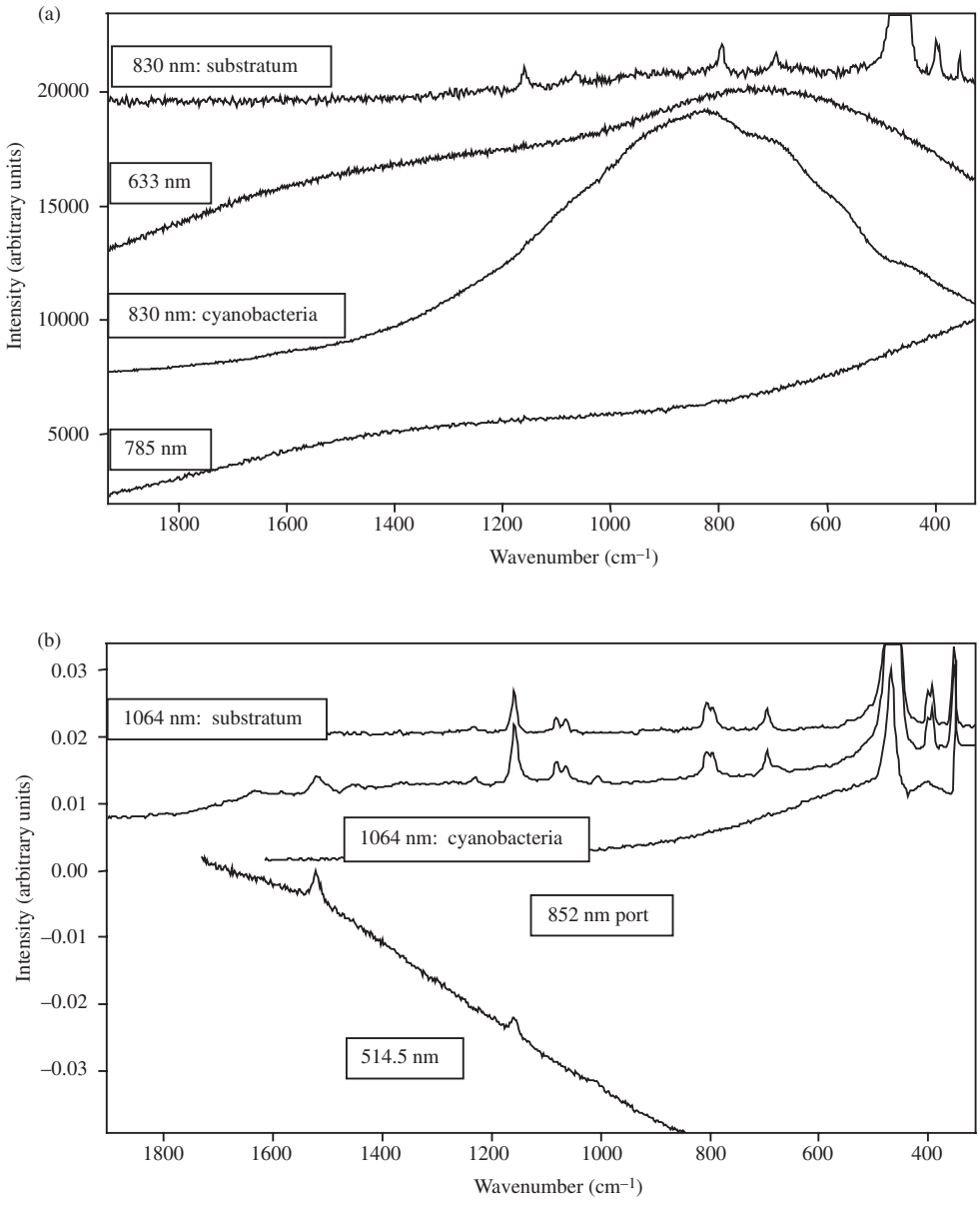

Fig. 6. (a) Stack plot of Raman spectra of *Chroococcidiopsis* collected using laser excitations of 633 nm (red), 785 nm (blue) and 830 nm (substratum and cyanobacterial layer). (b) Stack plot of Raman spectra of *Chroococcidiopsis* collected using laser excitations of 514.5, 852 nm portable (port) and 1064 nm (substratum and cyanobacterial layer).

as general markers of organic material (see Table 2a). This feature is a potential asset for detection of any relict biomolecules in the regolith profile of Mars buried beneath the oxidized surface zone. Bands elsewhere in the spectrum serve to define the more specific nature of the organic matter (and inorganic substratum) present (Wynn-Williams & Edwards 2000). The four corroborative bands at wavenumber shifts of 1590, 1549, 1323 and 1172 cm^{-1} shown in Table 4 that are characteristic of scytonemin are a good example of specific diagnosis in natural communities (Wynn-Williams *et al.* 1999). The 1064 nm system includes all of these organic bands, together with inorganic bands for minerals such as quartz and iron oxides composing the substratum itself, and is therefore more comprehensive in its diagnosis of the whole habitat. The miniaturization of the 1064 nm spectrometer is a major advance, not only for remote fieldwork in Antarctica and elsewhere, but also for incorporation into a future Mars mission to diagnose unknown biomolecules residual from any former communities that may have evolved during the wet Hesperian period 2.5–3.5 Gya (Wynn-Williams & Edwards 2000). A preliminary spectrum for *Acarospora chlorophana* pigments at 1064 nm excitation with a miniature Raman spectrometer fitted with an indium-gallium-arsenide (InGaAs) detector sensitive to infrared (outside the range of CCD detectors) is of similar quality to those of the laboratory system (Wynn-Williams *et al.* 2001), but is yet to be fully assigned. This enables spectra to be obtained from crustose lichens on immovable rock substrata before and after climate change or experimental manipulation of radiation fluxes. The non-intrusive nature of the analysis permits on-going

https://doi.org/10.1017/S147355040300123X Published online by Cambridge University Press

Table 6. *Raman wavenumbers and approximate vibrational assignments for cyanobacterial endolith*, Chroococcidiopsis sp. *and its sandstone substratum*

Excitation wavelength (nm)				
1064	852 port	830 substratum	514.5	Approximate assignment
2935 m, br				ν(CH) aliphatic
1633 w, br				
1585 vw				
1521 w, br			1518 s, br	ν(C═C) β-carotene
1450 vw, br				
1230 vw				α-quartz
1159 m		1160 mw		α-quartz/ν(C—C) β-carotene
			1155 br	ν(C—C) β-carotene
1081 mw, d				α-quartz
1064 mw, d		1066 w, br		α-quartz
1005 w			1006 mw	ν(C—C) aromatic
805 mw, d				α-quartz
795 mw, d		795 mw, br		Substratum
695 mw		695 w		α-quartz
679 w, sh				
464 vs	467 vs	465 vs		α-quartz
400 mw, d	400 ms, br	399 mw, d		α-quartz
393 mw, d		394 mw, d		α-quartz
354 m		355 mw		α-quartz
		320 w		
263 m		264 m		α-quartz
205 ms				α-quartz

Signal strength: vs = very strong; s = strong; mw = medium; w = weak; vw = very weak; br = broad band; sh = sharp.

experiments, and the fibre-optic flexibility of the detector head feeding the miniature spectrometer would permit long-term monitoring of microcosm experiments in laboratories that are distant from the macro Bruker instrument.

We conclude that the quality of Raman spectra from the laboratory 1064 nm spectrometer and the miniature field instrument fully justifies the selection of the infrared laser to optimize the signal-to-fluorescence ratio for biomolecules (especially pigments), despite the power loss at longer wavelengths.

Acknowledgements

The miniature Raman spectrometer and micro-imaging instrument is currently being funded by the NASA Mars Instrument Development Program (MIDP, NASA Grant NRA-97-16-OSS-049) to Dr David Dickensheets of Montana State University (Bozeman), in partnership with Dr Chris Schoen of Top Raman Inc. and Micron Optical Systems Inc, Norfolk, Virginia. We thank the University of Bradford for a Research Studentship to Emma Newton and Dennis Farwell for extensive technical support. We acknowledge the NASA Astrobiology Institute (especially Professor Baruch Blumberg, Director) for funding for the construction of the field version of the miniature Raman spectrometer for proposed use in Antarctica. David Wynn-Williams gratefully acknowledges support given by the British Antarctic Survey to the Antarctic Astrobiology Project in both the UK and Antarctica, and thanks the US National Science Foundation (especially the members of the Long Term Ecological Research site team) and USAP for Antarctic field support in the McMurdo Dry Valleys region; he also thanks the New Zealand Antarctic Research Programme for supporting his original collection of endolithic material, and especially Dr L. Greenfield of the University of Canterbury, New Zealand, who drew it to his attention.

References

Broady, P.A. (1996). Diversity, distribution and dispersal of Antarctic terrestrial algae. *Biodiversity Conservation* **5**, 1307–1335.

Buma, A.G.J., Van Hannen, E.J., Roza, L., Veldhuis, M. J. W. & Gieskes, W.W.C. (1995). Monitoring ultraviolet-B-induced DNA damage in individual diatom cells by immunofluorescent thymine dimer detection. *J. Phycology* **31**, 314–321.

Burke, C.M. & Burton, H.R. (1988). The ecology of photosynthetic bacteria in Burton Lake, Vestfold Hills, Antarctica. In *Biology of the Vestfold Hills, Antarctica*, eds Ferris, J.M., Burton, H.R., Johnstone, G.W. & Bayley, I.A.E., pp. 1–12. Kluwer, Dordrecht.

Chauhan, S., Pandey, R. & Singhal, G.S. (1998). Ultraviolet-B induced changes in ultrastructure and D1/D2 proteins in cyanobacteria *Synechococcus* sp. PCC 7942. *Photosynthetica* **35**, 161–167.

Cockell, C.S. & Knowland, J. (1999). Ultraviolet radiation screening compounds. *Biol. Rev. Camb. Phil. Soc.* **74**, 311–345.

Damste, J.S.S. & Koopmans, M.P. (1997). The fate of carotenoids in sediments: an overview. *Pure Appl. Chem.* **69**, 2067–2074.

Edwards, H.G.M. & Newton, E.M. (1999). Application of Raman spectroscopy to exobiological prospecting. In *The Search for Life on Mars*, ed. Hiscox, J.A., pp. 83–88. British Interplanetary Society, London.

Edwards, H.G.M., Holder, J.M. & Wynn-Williams, D.D. (1998). Comparative FT-Raman spectroscopy of *Xanthoria* lichen–substratum systems from temperate and Antarctic habitats. *Soil Biol. Biochem.* **30**, 1947–1953.

https://doi.org/10.1017/S147355040300123X Published online by Cambridge University Press

Edwards, H.G.M., Garcia-Pichel, F., Newton, E.M. & Wynn-Williams, D.D. (1999). Vibrational Raman spectroscopic study of scytonemin, the UV-protective cyanobacterial pigment. *Spectrochim. Acta A* **56**, 193–200.

Erokhina, L.G., Vishnivetskaya, T.A. & Gilichinskii, D.A. (1998). The content and composition of phycobilisome pigments in cells of ancient viable cyanobacteria from Arctic permafrost. *Microbiology* **67**, 682–687.

Friedmann, E.I. (1982) Endolithic microorganisms in the Antarctic cold desert. *Science* **215**, 1045–1053.

Friedmann, E.I., Hua, M.S. & Ocampo-Friedmann, R. (1988). Cryptoendolithic lichen and cyanobacterial communities of the Ross Desert, Antarctica. *Polarforschung* **58**, 251–259.

Haskin, L.A., Wang, A., Rockow, K.M., Jolliff, B.L., Korotev, R.L. & Viskupic, K.M. (1997). Raman spectroscopy for mineral identification and quantification for *in situ* planetary surface analysis: a point count method. *J. Geophys. Res. Planets* **102**, 19293–19306.

Hashimoto, S., Obata, K., Takeuchi, H., Needleman, R. & Lanyi, J.K. (1997). Ultraviolet resonance Raman spectra of Trp-182 and Trp-189 in bacteriorhodopsin: novel information on the structure of Trp-182 and its steric interaction with retinal. *Biochemistry* **36**, 11583–11590.

Holder, J.M., Wynn-Williams, D.D., Rull Perez, F. & Edwards, H.G.M. (2000). Raman spectroscopy of pigments and oxalates *in situ* within epilithic lichens: *Acarospora* from the Antarctic and Mediterranean. *New Phytologist* **145**, 271–280.

Huseby, B., Barth, T. & Ocampo, R. (1996). Porphyrins in Upper Jurassic source rocks and correlations with other source rock descriptors. *Organic Geochem.* **25**, 273–294.

Jahnke, L.S. (1999). Massive carotenoid accumulation in *Dunaliella bardawii* induced by ultraviolet A radiation. *J. Photochem. Photobiol. B* **48**, 68–74.

Kappen, L. (1993). Lichens in the Antarctic region. In *Antarctic Microbiology*, ed. Friedmann, E.I., pp. 433–490. Wiley-Liss, New York.

MacColl, R. (1998). Cyanobacterial phycobilisomes. *J. Structural Biol.* **124**, 311–334.

McKay, C.P. (1997). The search for life on Mars. *Origins Life Evol. Biosphere* **27**, 263–289.

Newton, E. (2001). FT-Raman spectroscopic characterisation of Antarctic lichen and cyanobacterial communities, Ph.D. thesis, University of Bradford.

Nienow, J.A., McKay, C.P. & Friedmann, E.I. (1988). Cryptoendolithic microbial environment in the Ross Desert of Antarctica: light in photosynthetically active region. *Microbial. Ecol.* **16**, 271–289.

Prouteau, P.J., Gerwick, W.H., Garcia-Pichel, F. & Castenholz, R. (1993). The structure of scytonemin, an ultraviolet sunscreen pigment from the sheaths of cyanobacteria. *Experientia* **49**, 825–829.

Rajagopal, S., Murthy, S.D.S. & Mohanty, P. (2000). Effect of ultraviolet-b radiation on intact cells of the cyanobacterium *Spirulina platensis*: characterization of the alterations in the thylakoid membranes. *J. Photochem. Photobiol. B* **54**, 61–66.

Russell, N. (1997). Temperate and Antarctic lichens: a FT-Raman spectroscopic study, Ph.D. thesis, University of Bradford.

Russell, N.C., Edwards, H.G.M. & Wynn-Williams, D.D. (1998). FT-Raman spectroscopic analysis of endolithic microbial communities from Beacon sandstone in Victoria Land, Antarctica. *Antarctic Sci.* **10**, 63.

Siebert, J., Hirsch, P., Hoffmann, B., Gliesche, C.G., Peissl, K. & Jendrach, M. (1996). Cryptoendolithic microorganisms from Antarctic sandstone of Linnaeus Terrace (Asgard Range): diversity, properties and interactions. *Biodiversity Conservation* **5**, 1337–1363.

Stransky, H. & Hager, A. (1970). The carotenoid pattern and the occurrence of the light-induced xanthophyll cycle in various classes of algae. IV. Cyanophyceae and Rhodophyceae. *Archiv Mikrobiol.* **72**, 84–96.

Vincent, W.F., Castenholz, R.W., Downes, M.T. & Howard-Williams, C. (1993). Antarctic cyanobacteria: light, nutrients and photosynthesis in the microbial mat environment. *J. Phycology* **29**, 745–755.

Wang, A., Joliff, B.L. & Haskin, L. (1999). Raman spectroscopic characterization of highly weathered basalt: igneous mineralogy, alteration products, and a microorganism. *J. Geophys. Res.* **104**, 27067–27077.

Wharton, R.A. (1994). Stromatolitic mats in Antarctic lakes. In *Phanerozoic Stromatolites*, vol. II, eds Bertrand-Sarfati, J. & Monty, C., pp. 53–70. Kluwer, Dordrecht.

Wynn-Williams, D.D. (2000). Cyanobacteria in deserts – life at the limit? In *The Ecology of Cyanobacteria: Their Diversity in Time and Space*, eds Whitton, B.A. & Potts, M., pp. 341–366. Kluwer, Dordrecht.

Wynn-Williams, D.D. & Edwards, H.G.M. (2000). Proximal analysis of regolith habitats and protective biomolecules *in situ* by laser Raman spectroscopy: overview of terrestrial Antarctic habitats and Mars analogs. *Icarus* **144**, 486–503.

Wynn-Williams, D.D. & Edwards, H.G.M. (2001). Strategies for protection from and avoidance of environmental UV radiation. *Lecture Notes in Physics* **42**, 245–260.

Wynn-Williams, D.D., Edwards, H.G.M. & Garcia Pichel, F. (1999). Functional biomolecules of Antarctic stromatolitic and endolithic cyanobacterial communities. *Eur. J. Phycol.* **34**, 381–391.

Wynn-Williams, D.D., Holder, J.M. & Edwards, H.G.M. (2000). Lichens at the limits of life: past perspectives and modern technology. *Bibliotheca Lichenologica* **75**, 275–288.

Wynn-Williams, D.D., Edwards, H.G.M. & Newton, E.M. (2001). The role of habitat structure for biomolecule integrity and microbial survival under extreme environmental stress in Antarctica (and Mars?): ecology and technology. In Proc. 1st Eur. Workshop on Exo/Astrobiology, Frascati, 21–23 May 2000, eds Ehrenfreund, P., Angerer, O. & Battrick, B. ESA SP-496, pp. 225–237.